Integrating Area-Selective Catalytic PMMA Etching with PMMA-Inhibited Area-Selective Deposition of HfO_2

Running title: ASD of HfO_2 using PMMA ASE walls

Running Authors: Novoselic et al.

Enzo Novoselic[1,a)], Natalya Tokranova[1], and Christophe Vallee[1]

[1]College of Nanotechnology Science and Engineering (CNSE), University at Albany, 257 Fuller Rd, Albany, New York 12203

[a)]Electronic mail: ejournetnovoselic@albany.edu

A fully self-aligned process integrating catalytic area-selective etching (ASE) of poly(methyl methacrylate) (PMMA) with PMMA-inhibited atomic layer deposition (ALD) of HfO_2 was developed and demonstrated at 300 °C. CoO_x was employed as a catalytic surface to promote the O_2-driven etching of PMMA, while SiO_2 does not show such behavior under identical conditions. In an oxygen atmosphere, PMMA on CoO_x exhibited temperature-dependent thinning consistent with catalytic activation, enabling selective polymer removal without photolithography. The inhibition of HfO_2 nucleation on PMMA increased strongly with temperature, extending the nucleation delay from fewer than 60 cycles at 200 °C to more than 190 cycles at 300 °C. Combining these two effects enabled a continuous, single-chamber sequence in which PMMA removal on CoO_x was followed by selective HfO_2 deposition. Ellipsometry and X-ray photoelectron spectroscopy confirmed 21 nm of HfO_2 growth on CoO_x and no measurable deposition on PMMA-covered SiO_2. The process represents an all-oxide, high-temperature area-selective deposition (ASD) route compatible with backend-of-line

materials and demonstrates the use of catalytic polymer etching to achieve lithography-free self-alignment.

I. INTRODUCTION

In Area-selective deposition (ASD), material is deposited only in certain areas (growth areas), while deposition is prevented in other areas (non-growth areas). In doing so, it enables continuation of an underlying pattern with different materials without requiring photolithography. As horizontal dimensions shrink and vertical stacking becomes more prevalent, conventional processing methods struggle with alignment issues and steep costs due to numerous lithography steps. As such, ASD is being adopted in an ever-increasing number of process flows in the semiconductor industry[1-4], resulting in both reduced alignment errors and lower processing costs.

The selective behavior at the core of ASD can be inherent – i.e., based on the bare, unmodified surfaces of the growth and non-growth areas. It can also be achieved through light surface modification to activate or deactivate specific areas. This can, for example, be achieved by depositing a layer of inhibitory chemistry on the non-growth areas[5-7], either through self-assembled monolayers, small-molecular inhibitors, or patterned blocking masks such as polymers. These processes, however, are rarely perfectly selective and are thus commonly supplemented by etch-back steps to significantly increase selectivity[8], or by more complex hybrid strategies[9]. Selectivity is typically measured in two forms: a selectivity ratio, measured as the ratio of the deposited thickness on the growth area to that of the non-growth area, and as the number of cycles before nucleation begins on the non-growth area[10,11].

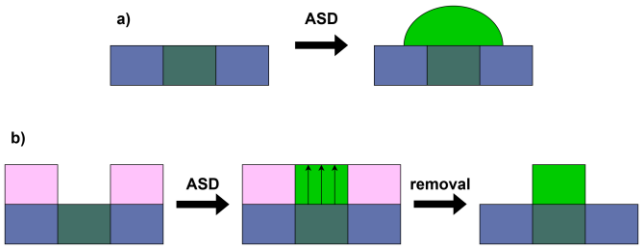

Fig. 1. Schematic of a) the mushrooming effect and b) prevention thereof using sidewalls.

But in the end, regardless of the approach used for ASD growth, there are still some issues. Chief amongst them is the emergence of a lateral growth phenomenon known as mushrooming. As the deposited thickness exceeds a certain threshold, the vertical surfaces of the newly deposited material become growth areas. This causes growth perpendicular to the target growth direction, resulting in mushroom-like film morphology[12,13], as shown in Figure 1a. This behavior has historically limited the usefulness of ASD, as the threshold thickness is typically on the order of a few nanometers. To raise the threshold thickness, several methods have been developed. This includes techniques such as a polymer wall-based process introduced by Sinha et al.[7], further refined by Zhang et al.[14] to be self-aligned, and a selectively deposited thiolate multilayer-based process by Shearer et al.[15] These walls constrain growth to the vertical dimension, thus preventing mushrooming, as shown in Figure 1b.

In Zhang et al.'s process, a uniform polymer is deposited over the entire surface, and then selectively removed from the growth areas using area-selective etching (ASE).[14] This can be achieved through polymer etching via selective catalysis of an etchant gas[14,16,17], or through polymer lift-off by selective etching of a single surface layer from the growth areas[18]. This builds upon electron-beam induced selective etching, first demonstrated over 35 years ago[19], which had remained unused due to being assisted rather than self-aligned. Similarly, catalytically driven processes were first shown for self-aligned deposition almost 35 years ago[20], but remained absent

from the etching space. The remaining hurdle to the adoption of selective etching in the industry is turning it from an academic curiosity into a valuable process for chip making. Doing so requires, amongst other things, compatibility with industry-relevant materials.

In previous results[14,16,17], various materials were used as catalytic surfaces, including semiconductor fabrication-relevant materials such as Ti, Cu, Ru, and Co, a material that is seeing use in BEOL processing[21-25]. Cobalt oxide has long been used in oxygen-based catalyzation processes[26], and was thus chosen as the target of our experiments over metallic Co. It is important to note that metallic Co has been shown to cause etching of poly(lactic acid) under H_2 and N_2 atmospheres[17], but has not been used in O_2 atmospheres, as it would readily oxidize in such conditions. Furthermore, the observed catalytic capabilities of Co are likely to be due to the native CoO_x rather than the metallic Co itself, as the authors of that study note. In cobalt oxide, this is primarily achieved through its two oxidation states, Co^{2+} and Co^{3+}, which enable it to readily supply or accept electrons as needed for catalytic processes.

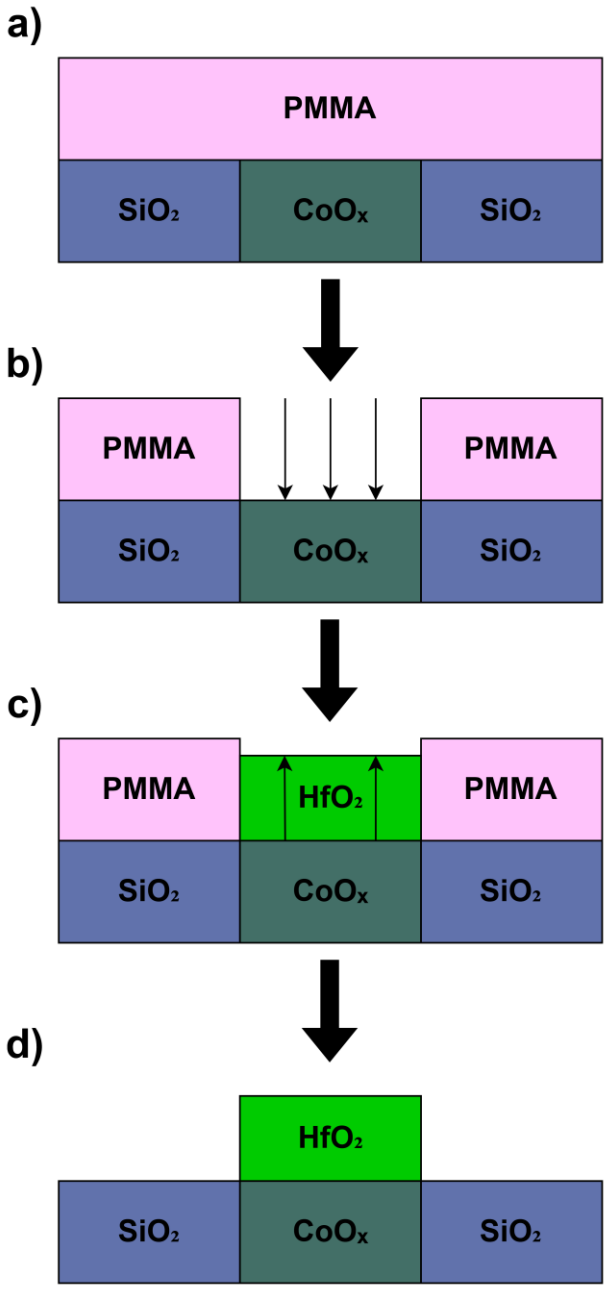

Fig. 2. Schematic of the self-aligned ASD of HfO_2 using PMMA etched by ASE. (a) The PMMA is deposited onto the surface. (b) The PMMA is selectively etched from the CoO_x areas using catalytic etching. (c) HfO_2 is deposited on the CoO_x in the opening left by the ASE. (d) The PMMA is removed from the surface, resulting in a self-aligned HfO_2 deposition on CoO_x.

In this paper, we studied the ASE of poly(methyl methacrylate) $(C_5H_8O_2)_n$ (PMMA), alongside the ASD of HfO_2 on non-PMMA-covered surfaces. We investigated the use of cobalt oxide (CoOx) as a catalyst for PMMA removal and thus as a growth area compared with SiO_2. Combining these two processes should result in a selectively deposited HfO_2 film on cobalt oxide without mushrooming as shown in Figure 2.

II. EXPERIMENTAL

A. Substrate preparation and CoO_x deposition

Samples were prepared on silicon wafers covered with a thermal oxide layer. A 26-nm-thick CoO_x film was deposited via plasma-enhanced atomic layer deposition (PEALD) in an Oxford FlexAL system. Cobaltocene [$Co(C_5H_5)_2$, Strem Chemicals] was used as the cobalt precursor with O_2 plasma as the co-reactant. The PEALD cycle consisted of three precursor doses (each with a 2s pulse and a 3s purge), followed by a 2s plasma setup step, a 5s ICP plasma (300 W), and a final 8s purge. This resulted in a growth per cycle (GPC) of 0.5 Å.

The photoresist pattern was created on the CoO_x film using photolithography. A 3 nm SiO_2 layer was subsequently deposited via room-temperature reactive sputtering. Following photoresist lift-off, the resulting substrates consisted of alternating regions of exposed CoO_x and SiO_2-covered CoO_x. Surface features were verified using a Keyence VK-X3000 3D surface profilometer with 5x and 50x objective lenses.

B. PMMA deposition and area-selective etching

Polymethyl methacrylate (PMMA) thin films were spin-coated using a 2% solution of 495,000 MW PMMA in anisole as sold under the “495 PMMA A2” label [MicroChem]. The

solution was spun at 10,000 rpm for 60 s (1,000 rpm/s ramp) and subsequently baked at 175 °C for 1 h to enhance thermal stability[27]. This produced nominal thicknesses of 60 nm on blanket CoO_x and 50 nm on blanket SiO_2.

Precise control of the initial PMMA thickness was achieved by uniform thinning using a 10-W, 10-mTorr O_2 plasma. Self-aligned PMMA patterning via area-selective etching (ASE) was investigated by exposing the patterned samples to 230 mTorr O_2 at various temperatures. Etching rates and PMMA thickness changes were monitored in real-time using an in-situ eight-wavelength ellipsometer (FilmSense FS-1EX) integrated into the FlexAL system and then confirmed using an ex-situ J.A. Woollam M-2000 ellipsometer.

C. Area-selective deposition of HfO_2 and characterization

Area-selective deposition (ASD) of HfO_2 was performed via thermal ALD using tetrakis(dimethylamino)hafnium (TDMAHf) and H_2O. A single ALD cycle comprised a 1 s precursor pulse, a 3 s precursor purge, a 20 ms H_2O pulse, and an 8 s co-reactant purge. The process was repeated for up to 200 cycles.

The HfO_2 growth was monitored in situ using the FilmSense ellipsometer. Post-deposition thickness characterization was performed using the ex-situ ellipsometer. Chemical composition and film purity were analyzed via X-ray photoelectron spectroscopy (XPS) in a PHI Quantera Hybrid system equipped with a monochromatic Al Kα source. Low-resolution surveys were collected with a binding energy range of 0-1100 eV at a pass energy of 280 eV.

III. RESULTS AND DISCUSSION

A. Area Selective etching (ASE) of PMMA

The catalytic effect of CoO_X, as opposed to SiO_2, was investigated by first exposing a PMMA film deposited on both SiO_2 and CoO_X substrates to a 230 mTorr O_2 atmosphere at different substrate temperatures for 30 minutes. The real-time thickness evolution for both substrates is plotted in Figure 3.

Figure 3a shows the thickness evolution with time for PMMA deposited on SiO_2 and exposed to O_2 gas at various temperatures. The initial PMMA thickness was 50 nm. The thickness does not change significantly over time at 250 and 300 °C, with only 0.4 nm lost at 300 °C, corresponding to a thickness reduction of less than 1%. A more significant reduction is observed for T = 350 °C, with ~2.5% thickness lost after 30min. This result was expected, since SiO_2 has previously been shown to have no catalytic oxygen-dissociation properties[14]. The thickness reduction at 350 °C is attributed to the polymer's thermal degradation rather than to a weak catalysis effect. The PMMA starts to degrade at 350 °C, indicating an upper bound of 300°C for our processing temperature. This falls in line with previous results[28-30], whereby a range of 300~400 °C has been measured for the rapid thermal degradation of PMMA.

The thickness evolution with time for PMMA deposited on CoO_x is shown in Figure 3b. The initial PMMA thickness was 60 nm. At all temperatures, we observe a time-dependent thickness loss (etching), increasing from ~6% after 30 min at 250 °C to ~50% after 30 min at 350 °C. The minimal etching at 250 °C indicates that this temperature is close to the threshold temperature needed for the catalytic dissociation of O_2 by CoO_x. The substantial decrease in thickness over time is clear experimental evidence of the catalytic dissociation of O_2 at the CoO_x

surface and of PMMA etching by O* radicals. This result is in good agreement with the literature since cobalt oxides have been reported as catalysts in various oxygen-based processes.[26,31] At 350 °C, the maximum etching rate (not linear with time) for this process is obtained, around 1 nm/min.

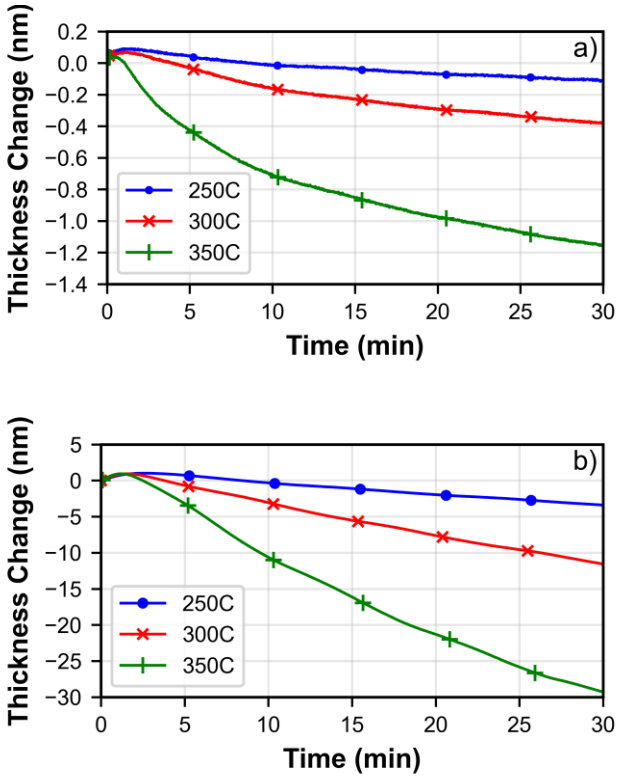

Fig 3. Evolution of the thickness of PMMA when subjected to an O_2 atmosphere on a) SiO_2, and b) CoO_x.

B. O_2 Plasma etching of PMMA

In addition to the selective catalytic etching of PMMA, we also studied the O_2 plasma etching of PMMA. Our PMMA spin-coating process does not permit deposition of an ultrathin PMMA film (<10 nm), and 60 nm is the minimum film thickness that can be deposited on CoO_x. With a maximum etching rate of 1nm/min obtained at 350°C, this means that etching all PMMA

requires at least 1 hour of processing time. To speed up the process and reduce the time during which the PMMA is exposed to high temperatures on SiO_2 surfaces, we decided to add an O_2 plasma etching step before the ASE process. Since PMMA is known to etch very quickly in O_2 plasma, we intentionally ignited the plasma with only 10W of ICP power to limit O_2 dissociation, thereby reducing the etching rate and better controlling it. Figure 4 shows the PMMA etching with time on SiO_2 for 10W O_2 plasma and a substrate temperature of 300 °C. A nearly linear time-dependent etch rate is observed, resulting in an etch rate of 6 nm/s (360 nm/min), which is 360 times the etch rate obtained from catalytic etching with O_2.

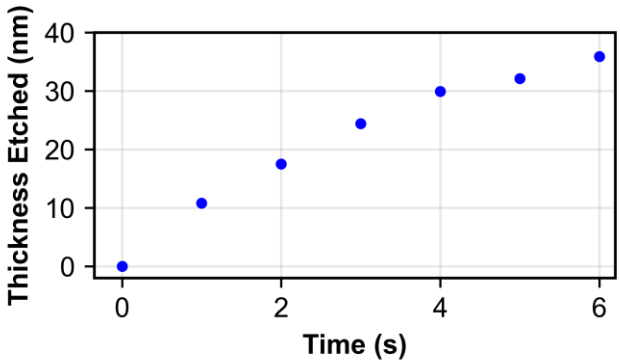

Fig 4. Evolution of the thickness of the PMMA when exposed to an O_2 plasma.

To confirm that the plasma thinning did not affect the polymer chemistry in a way that would render the catalytically driven etching ineffective, we then exposed the remaining PMMA after the O_2 plasma on SiO_2 and CoO_x surfaces to an oxygen atmosphere at ASE conditions. The result obtained after this exposure is nearly identical to that shown in Figure 3. This indicates that the O_2 plasma exposure does not induce any changes in the PMMA that could alter the ASE process. This falls in line with our expectations, as the plasma-based thinning employs O* radicals to etch the film from the top surface, which is the same process as our catalytic etching,

which employs O* radicals to etch the film from the interface. However, it was necessary to verify that other plasma constituents, such as vacuum ultraviolet photons, did not negatively affect the catalytic process[32,33].

C. Temperature-driven inhibition of HfO_2 on PMMA

After the first step of ASE, the remaining PMMA on SiO_2 surfaces must act as an inhibitor of the ASD of HfO_2 on CoO_x. Figure 5 shows the real-time evolution of the thickness of HfO_2 deposited by ALD on untreated PMMA over 200 cycles at various substrate temperatures, as measured with the in-situ ellipsometer. This figure shows that PMMA can effectively block HfO_2 growth, but the inhibiting property, i.e., the nucleation delay, is substrate temperature-dependent, ranging from ~50 cycles at 150 °C to more than 190 cycles at 300 °C. The numbers agree with Brummer et al., who found around 60 cycles of nucleation delay using the same TDMAHf precursor and PMMA at 200 °C[34]. Increasing the substrate temperature results in a significantly extended nucleation delay (and thus selectivity).

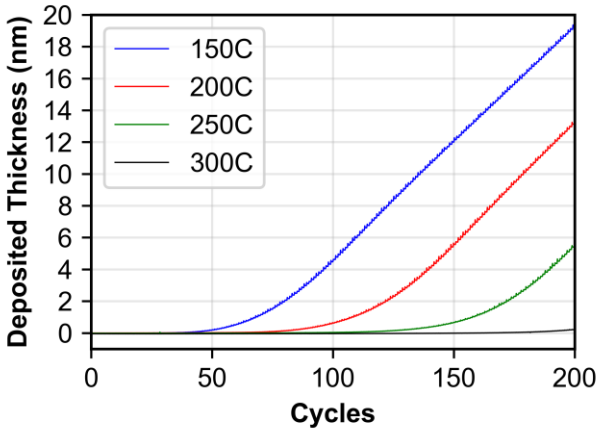

Fig 5. Growth of HfO_2 on PMMA at various temperatures.

Most ASD processes that use inhibitors, such as Self-Assembled Monolayers (SAMs), Small Molecule Inhibitors (SMIs), or polymers, exploit their hydrophobic nature to hinder ALD nucleation. Regarding PMMA, many groups reported a blocking effect during ALD thanks to its hydrophobicity[35,36]. Our first hypothesis to explain the nucleation delay behavior as a function of temperature was that the degree of hydrophobicity is enhanced with temperature. To verify it, we studied the film composition by XPS and its hydrophobicity using water contact angle. The objective was to determine whether chemical changes at the surface or changes in the film's hydrophobic properties with temperature can explain the modification in PMMA's blocking properties.

Figure 6 shows the XPS C1s peak for untreated PMMA samples annealed in an inert atmosphere at various temperatures. The shape of this peak is the sum of four chemical states: C−C/C-H near 284.8−285 eV, C in the α-position to the ester group near 285.7−285.85 eV, C−O near 286.9 eV, and O−C=O near 289 eV[37]. There is no clear experimental evidence of a chemical modification of the surface with respect to annealing temperature, such as a significant increase in the nonpolar C-C and C-H bonds relative to the polar C-O bonds.

Figure 7 shows the water contact angle (WCA) for the XPS-analyzed samples. A slight increase in WCA is observed as a function of the annealing temperature, which correlates with the nucleation delay increase observed in Figure 5. Although XPS analysis shows no change in the material's chemical composition, this increase in hydrophobic properties can be explained by surface rearrangement facilitated by increased chain mobility. During annealing, the polymer chains gain sufficient mobility to minimize surface energy when exposed to air; consequently, the hydrophilic polar groups reorient inward while nonpolar groups, characterized by C-H bonds, migrate toward the surface to interact more favorably with the ambient environment. This

reorientation modifies the polymer's hydrophobicity without altering its chemical identity. Notably, the contact angle decreased gradually after the initial measurement—likely due to water entering and wetting the polymer matrix—therefore, measurements should be performed as quickly as possible after droplet contact at room temperature to minimize wetting effects.

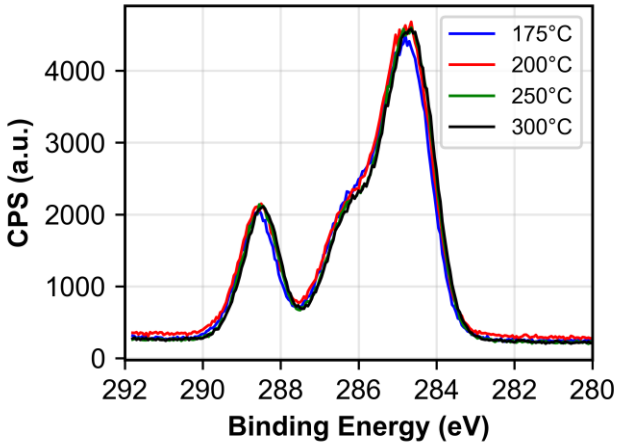

Fig 6. C1s XPS Peak for PMMA annealed at various temperatures.

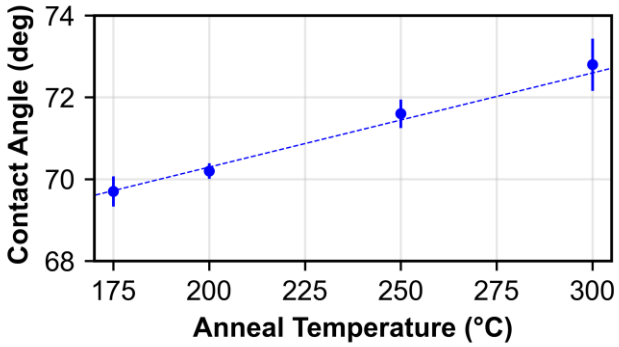

Fig 7. Water contact angle for PMMA annealed at various temperatures.

However, the change in hydrophobicity appears too minor to be a sufficient explanation for the increase in nucleation delay. Furthermore, annealing a sample of PMMA to 300°C, then cooling it down to 150°C to perform the deposition, results in the same nucleation delay as the

sample that had the deposition done at 150°C without prior annealing, thus likely disproving the above hypothesis.

A stronger hypothesis is that the nucleation delay is correlated with an increase in desorption following an Arrhenius model, as higher temperatures favor the desorption of precursor molecules. As can be seen in Figure 8, which shows the Arrhenius plot for the nucleation delay, the observed behavior strongly follows the hypothesis.

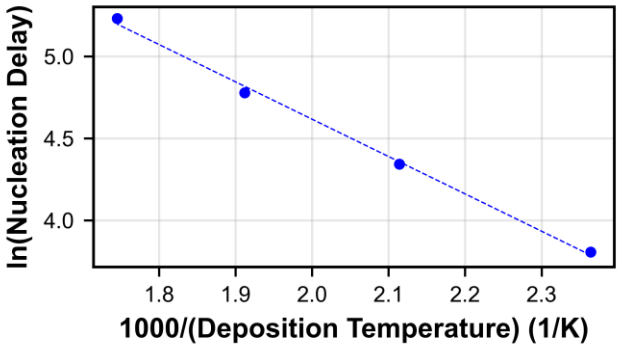

Fig8. Arrhenius plot of the nucleation delay as a function of deposition temperature.

This thermal effect, combined with the observed growth behavior, suggests that HfO_2 deposition on the polymer initiates via island-type growth. In this regime, growth is restricted to specific defect sites where precursor molecules can adsorb and react to form nuclei. As the thermal energy of the precursor increases with temperature, the statistical likelihood of desorption upon reaching these defect sites also increases, thereby delaying the transition to steady-state growth. This behavior, characterized by an initially low growth per cycle (GPC) that gradually increases as nuclei merge into a continuous layer, aligns with the theoretical framework reported by Mameli et al.[38] for passivated silicon surfaces.

D. ASD of HfO_2 on CoO_x and SiO_2 vs PMMA

The ALD of HfO_2 is studied on CoO_x, SiO_2, and untreated PMMA substrates using in situ ellipsometric measurements. HfO_2 thickness as a function of ALD cycles is plotted in Figure 9 for all substrates at the deposition temperature of 300°C. For both SiO_2 and CoO_x substrates, linear growth is observed with no nucleation delay. On the PMMA substrate, HfO_2 growth is inhibited for 200 cycles. However, to verify the blocking properties of the PMMA, the chemical composition of the PMMA samples after 200 HfO_2 ALD cycles was analyzed by XPS (see Table 1). The XPS analysis shows traces of HfO_2 at the PMMA surface, with the presence of a Hf4f peak (0.47 at%).

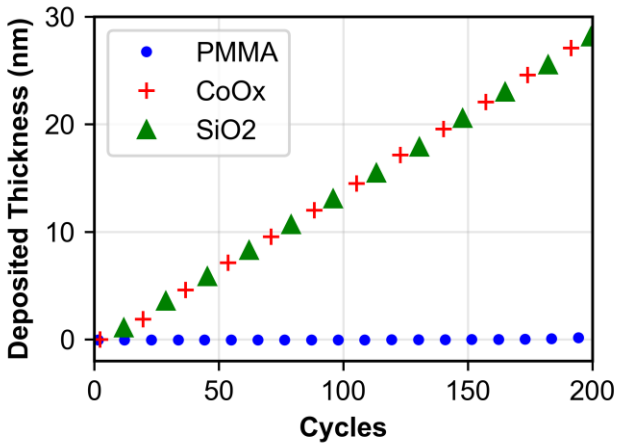

Fig 9. Growth of HfO_2 on various substrates at 300°C.

Table I. XPS of surface composition on top of PMMA film after 200 cycles of HfO_2.

	C	O	Si	Hf
Atomic %	74.08	22.91	2.54	0.47

E. ASE + ASD process

Figure 10 shows the selective growth behavior of HfO_2 deposited by ALD at 300°C on CoO_x and SiO_2 surfaces after the selective etching of PMMA was done. The etching consisted of a 10W O_2 plasma etching for 7s to reduce the thickness from approximately 55 nm to 20 nm, followed by 60 minutes of exposure in an O_2 atmosphere at 230 mTorr for the catalytic etching. Since ASE and ASD processes are carried out in sequence in the ALD chamber, the substrate temperature is the same for both processes and is fixed at 300°C.

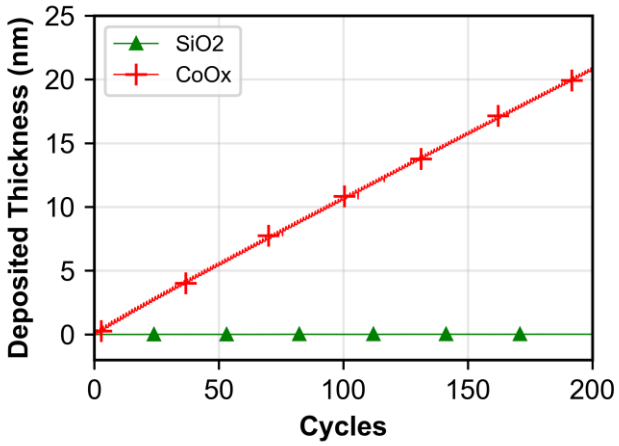

Fig 10. Growth of HfO_2 following ASE on CoO_x and SiO_2.

As shown in Figure 10, 21 nm of HfO_2 is deposited on CoO_x, whereas no HfO_2 appears to be deposited on the SiO_2 surface inhibited with PMMA. This indicates that we have successfully used the ASE process to selectively remove PMMA from the cobalt oxide surface without removing it from the SiO_2 surface, thereby enabling ASD growth by ALD on CoO_x vs SiO_2. After the ASD process, the PMMA on the SiO_2 surface is removed by dissolving it in acetone.

The ASE+ASD process was finally done on patterned samples, with two different pattern areas. One contains alternating lines with widths between 500 and 540 μm, whilst the other

contains a single 81 µm-wide line. Figure 11 shows top-view images of the patterns before the PMMA Deposition (11a and 11b), after the ASE process (11c and 11d), and after the ASD process (11e and 11f). As shown, the dimensions remain constant throughout the process, indicating that we are successfully transferring the pattern. The measurement error, measured as the width of an image pixel, is ±5 µm for the ~500 µm lines, and ±500 nm for the ~80 µm lines. All measurements were thus rounded to the nearest multiple of 500nm and 5µm, respectively.

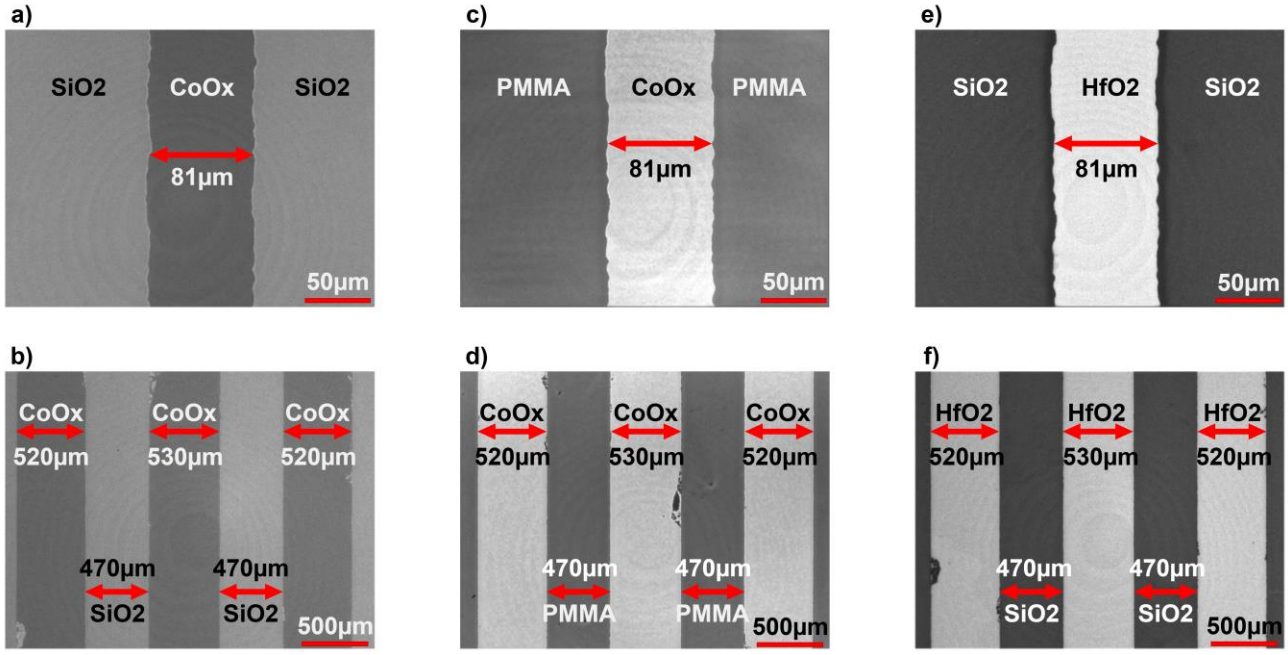

Figure 11. Top view image of line profiles after a) b) SiO_2 patterning, c) d) PMMA ASE, e) f) HfO_2 ASD + PMMA removal.

Finally, we must remember that the objective of this study was to achieve a combination of selective etching via catalysis and selective deposition via inhibition and ALD, to selectively grow HfO_2 without mushrooming. AFM measurements have been made to verify the verticality of the selectively deposited film. As shown in Figure 12, we observe a roughly 100nm exclusion zone with no growth between the ALD film and the polymer, as first reported by Vervuurt et al.[39], albeit much narrower than in their study. This may be due to the low thickness of the

PMMA used in this study, as discussed by Hahn[40]. It can also be seen that the PMMA's edge shows reflow, with a slope width of about 150nm. Furthermore, due to the exclusion zone, the PMMA was unable to perform its intended function as a wall, resulting in a non-vertical deposition sidewall for the HfO_2.

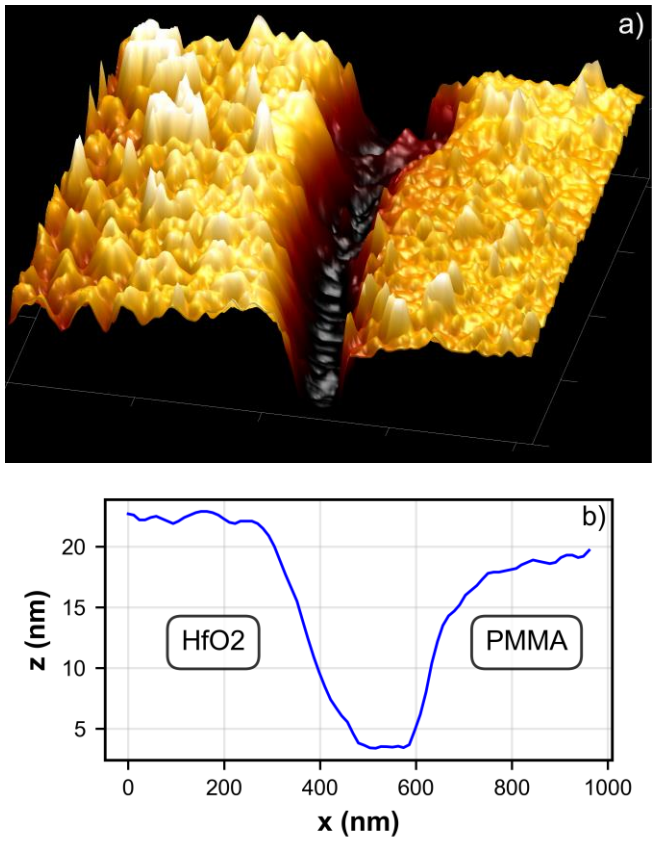

Figure 12. a) AFM 3D map of pattern after HfO_2 deposition, and b) line scan taken from the center of the 3D map.

IV. Conclusion

A self-aligned HfO_2-on-CoO_x deposition method was demonstrated. By leveraging the catalytic properties of CoO_x, a self-aligned PMMA layer was formed on the patterned CoO_x/SiO_2 samples, which was then used as an inhibiting layer for HfO_2 ASD by ALD. We further demonstrated that PMMA's blocking capacity increases with temperature until a degradation

regime is reached. This behavior appears to be well explained by an Arrhenius law governing the desorption of physisorbed precursor molecules at the polymer surface. It has been demonstrated that, by using PMMA, all process steps can be performed in a single reactor at the same temperature without any vacuum break: plasma thinning, Area Selective Etching by catalytic effect, and Area Selective Deposition. However, challenges remain due to an exclusion zone and non-negligible polymer reflow, which prevent extending this process as-is to the nanometer scale. Further studies should be conducted to identify suitable polymers for the task.

ACKNOWLEDGMENTS

This work was funded by Tokyo Electron Limited and the New York State CATN2 program through the TEL plasma scientist innovation grant.

AUTHOR DECLARATIONS

Conflict of Interest

The authors have no conflicts to disclose.

DATA AVAILABILITY

The data that support the findings of this study are available within the article.

REFERENCES

[1]J.-O. Carlsson, Crit. Rev. Solid State Mater. Sci. **16**, 161–212 (1990).

[2]G.N. Parsons, and R.D. Clark, Chem. Mater. 32, 4920–4953 (2020).

[3]S. Lee, G. Lee, J. Oh, and J. An, Int. J. Precis. Eng. Manuf. **26**, 2551–2571 (2025).

[4]T.-L. Liu, and S.F. Bent, Mater. Horiz. 12, 1711–1725 (2025).

[5]J. Petermann, T. Hoffmann, and J. Martinez-Salazar, J. Vac. Sci. Technol. B **12**, 613–615 (1994).

[6]D. Davazoglou, S. Vidal, and A. Gleizes, in *MMN 2000*, (2001), pp. 131–134.

[7]A. Sinha, D.W. Hess, and C.L. Henderson, J. Electrochem. Soc. **153**, G465 (2006).

[8]R. Vallat, R. Gassilloud, B. Eychenne, and C. Vallée, J. Vac. Sci. Technol. A **35**, 01B104 (2017).

[9]C. de Paula, D. Bobb-Semple, and S.F. Bent, J. Mater. Res. **36**, 582–591 (2021).

[10]G.N. Parsons, J. Vac. Sci. Technol. A **37**, 020911 (2019).

[11]C.T. Nguyen, E.-H. Cho, B. Gu, S. Lee, H.-S. Kim, J. Park, N.-K. Yu, S. Shin, B. Shong, J.Y. Lee, and H.-B.-R. Lee, Nat. Commun. **13**, 7597 (2022).

[12]R.H.A. Ras, E. Sahramo, J. Malm, J. Raula, and M. Karppinen, J. Am. Chem. Soc. **130**, 11252–11253 (2008).

[13]N.M. Carroll, and G.N. Parsons, J. Vac. Sci. Technol. A **42**, (2024).

[14]C. Zhang, M. Leskelä, and M. Ritala, Coatings **11**, 1124 (2021).

[15]A. Shearer, Y. Cho, M. Kim, A. Werbrouck, T.-L. Liu, C.J. Takacs, B. Shong, and S.F. Bent, ACS Nano **19**, 11936–11948 (2025).

[16]V. Lasonen, A. Vihervaara, G. Popov, E. Tois, L. Mester, M. Karimi, Y. Ilarionova, R. Jafari Jam, J. Sundqvist, and M. Ritala, Chem. Mater. **35**, 6097–6108 (2023).

[17]V. Lasonen, V. Rajamäki, M. Chundak, E. Tois, S. Hietala, and M. Ritala, Chem. Mater. **36**, 11645–11655 (2024).

[18]A.T. Mohabir, G. Tutuncuoglu, T. Weiss, E.M. Vogel, and M.A. Filler, ACS Nano **14**, 282–288 (2020).

[19]S. Matsui, T. Ichihashi, and M. Mito, J. Vac. Sci. Technol. B **7**, 1182–1190 (1989).

[20]K. Tsubouchi, and K. Masu, J. Vac. Sci. Technol. A **10**, 856–862 (1992).

[21]M.J.M. Merkx, and A.J.M. Mackus, AtomicLimits, (2022).

[22]L.-J. Wei, Z.-H. Zhou, Y.-W. Wu, M. Li, and S. Wang, J. Electrochem. **28**, 12 (2022).

[23]A.E. Rogozhin, and O.G. Glaz, Russ. Microelectron. **53**, 102–116 (2024).

[24]L. Jin, Z.-Y. Wang, and F.-Z. Yang, J. Electron. Mater. **54**, (2025).

[25]T. Jiang, and H. Hu, Electronics **14**, 894 (2025).

[26]S. Gupta, R. Fernandes, R. Patel, M. Spreitzer, and N. Patel, Appl. Catal. A Gen. **661**, 119254 (2023).

[27]C. Cao, Z. Tan, S. Sun, Z. Liu, and H. Zhang, Polym. Degrad. Stab. **96**, 2209–2214 (2011).

[28]N. Grassie, and H.W. Melville, Proc. R. Soc. Lond. **199**, 14–23 (1949).

[29]E. Giannetti, R. Mazzocchi, L. Fiore, and F. Visani, J. Polym. Sci. A Polym. Chem. **24**, 2517–2551 (1986).

[30]L.E. Manring, Macromolecules **24**, 3304–3309 (1991).

[31]C. Alex, S.C. Sarma, S.C. Peter, and N.S. John, ACS Appl. Energy Mater. **3**, 5439–5447 (2020).

[32]H. Shinohara, T. Kasahara, S. Shoji, and J. Mizuno, J. Micromech. Microeng. **21**, 085028 (2011).

[33]G.S. Oehrlein, R.J. Phaneuf, and D.B. Graves, J. Vac. Sci. Technol. B **29**, 010801 (2011).

[34]A.C. Brummer, A.T. Mohabir, D. Aziz, M.A. Filler, and E.M. Vogel, Appl. Phys. Lett. **119**, 142901 (2021).

[35]E. Färm, M. Kemell, M. Ritala, and M. Leskelä, J. Phys. Chem. C **112**, 15791–15795 (2008).

[36]M.A. Forte, R.M. Silva, C.J. Tavares, and R.F.E. Silva, Polymers (Basel) **13**, 1346 (2021).

[37]K.T. Young, A. Hsiao, A. Brummer, and C. Yang, J. Phys. Chem. C **128**, 14790–14800 (2024).

[38]A. Mameli, B. Karasulu, M.A. Verheijen, B. Barcones, B. Macco, A.J.M. Mackus, W.M.M.E. Kessels, and F. Roozeboom, Chem. Mater. **31**, 1250–1257 (2019).

[39]R.H.J. Vervuurt, A. Sharma, Y. Jiao, W.E.M.M. Kessels, and A.A. Bol, Nanotechnology **27**, 405302 (2016).

[40]L. Hahn, presented at the RAFALD 2025 Conference, Grenoble, France, 2025 (unpublished).